Macromolecules **2009**, *42*, 1331−1343

Influence of Interfacial Layer Between Nanoparticles and Polymeric Matrix on Viscoelastic Properties of Hydrogel Nanocomposites

Masaki Yanagioka,[†] **Michael F. Toney,**[‡] **and Curtis W. Frank***[,†]

Department of Chemical Engineering, Stanford University, Stanford, California 94305, and Stanford Synchrotron Radiation Laboratory, Stanford Linear Accelerator Center, Menlo Park, California 94025

Received September 22, 2008; Revised Manuscript Received December 9, 2008

ABSTRACT: The viscoelastic properties of nanocomposites are influenced by both the nanoparticle distribution and the nanoparticle−polymer affinity. These two parameters are closely coupled, and evaluation of individual contributions to the mechanical properties is a critical requirement for efficient development of nanocomposites. To decouple these two effects, we utilized charge repulsion among nanoparticles so that we could essentially eliminate particle agglomeration. We then investigated how the nanoparticle−polymer affinity relates to the mechanical properties of the nanocomposite by comparing silica and polystyrene nanoparticles. The surface roughness of the particles and the molecular conformation of the interfacial layer between the polymer and the nanoparticles were characterized by synchrotron small-angle X-ray scattering and quartz crystal microbalance, respectively. On polystyrene particles, the surface roughness was larger, and the polymer adsorbed strongly. Consequently, the mobility of the adsorbed polymer was reduced compared to that on silica particles. This reduced mobility explains a smaller viscoelastic loss for the polystyrene-filled nanocomposite compared to the silica-filled nanocomposite.

1. Introduction

Viscoelastic properties of nanocomposites are known to be dependent on properties of the embedded particles, such as affinity of the particles to the matrix polymer, the particle size, and the dispersion of the particles within the matrix.[1] The effects of particle dispersion and their affinity to the matrix polymer are tightly coupled and, thus, understanding of the viscoelastic behavior of nanocomposites is still limited. This poses a significant barrier against efficient and rapid development of nanocomposites with desired mechanical properties, which can be used, for example, in numerous automotive, aerospace, and biological applications.[2−5]

To overcome this challenge, one needs to decouple the effects of particle agglomeration and the particle−polymer affinity to estimate each contribution to the overall mechanical properties of nanocomposites. One way to approach this is with the polymerized crystalline colloidal array (PCCA) developed by Asher et al.,[6−13] where colloidal particles repel each other due to the reduced concentration of counter-ions that screen surface charge on the particles. This array may be encapsulated within a polymeric matrix without changing the interparticle distance. The PCCA diffracts visible light, and the interparticle distance is determined through Bragg's law simply by measuring an extinction spectrum.[14]

Ford et al. utilized the PCCA using poly(methylacrylate) elastomers as the polymeric network and 3-(trimethoxysilyl)propyl methacrylate coated silica particles as the filler.[15−17] In these nanocomposites, the functionalized silica particles were chemically cross-linked with the polymeric matrix. They studied the effects of the silica dispersion on the reinforcement of the filled composites, when the samples were in uniaxial or equi-biaxial deformation, and demonstrated that the aggregated silica particles in the nanocomposites led to higher extensibility and lower Young's modulus of the filled nanocomposites, compared to the one that had ordered particle distribution.

Inspired by these publications, we previously synthesized ordered and random silica-filled hydrogels, and evaluated the effect of particle agglomeration on the dynamic mechanical properties of the filled hydrogels.[18] This composite system enabled us to decouple the effects due to particle distribution and particle−polymer affinity. We showed that eliminating particle agglomeration in the nanocomposite led to a higher Young's modulus due to the increased contact area between the particles and the matrix polymer. In addition, we demonstrated that the interparticle distance in the filled hydrogel was determined from the interaction potential calculated by the Derjaguin−Landau−Verwey−Overbeek (DLVO) theory.

In this article, we further investigate not only the effect of particle distribution on mechanical properties, but also the influence of the particle−polymer affinity by varying the type of particle. It should be emphasized that we can eliminate the effect of particle distribution even with different particles, because the interparticle distance is monitored separately using the Bragg diffraction peak. We selected silica and polystyrene particles as model particles possessing hydrophilic and hydrophobic surfaces, respectively, and expected that different affinities of these particles to the matrix polymer should lead to different molecular conformations of the polymer chains adsorbed on the particles.

There have been early efforts to determine the transition-layer thickness in polymer blends using line broadening of NMR spectra or the Raman band associated with the so-called longitudinal acoustic mode.[19,20] A more recent and powerful approach to investigate colloidal particles[21−23] and their diffuse interfacial layers is synchrotron small-angle X-ray scattering (synchrotron SAXS).[24−28] Some of its major advantages are a broad spatial range from submicron to atomic length scales, capability to probe the internal structure of particles,[29−31] *in situ* measurement,[32] and freedom from multiple scattering. A synchrotron source creates an intense and highly collimated X-ray beam (that is made monochromatic) so that the acquisition time can be short.[33] This feature expedites studies of weakly scattering systems. In practice, synchrotron SAXS allows us to measure the transition-layer thickness based on the electron density profile and the deviation from the classical Porod's Law.[34,35]

---

* Corresponding author. E-mail: curt.frank@stanford.edu.

[†] Department of Chemical Engineering, Stanford University.

[‡] Stanford Synchrotron Radiation Laboratory, Stanford Linear Accelerator Center.

10.1021/ma802152s CCC: $40.75

The quartz crystal microbalance with dissipation monitoring (QCM-D) method gives more information about the adsorbed polymeric layer on a substrate. It is a sensitive technique that detects a small amount of adsorbed substance on an oscillating quartz crystal. Coating the crystal with either silicon dioxide or polystyrene provides a model system where we can monitor the adsorption of polymer chains on each surface. Proper modeling of the adsorption behavior allows us to determine not only the thickness of the adsorbed layer, but also its viscoelastic properties. The classical Sauerbrey model[36] is only valid for rigid layers, and soft layers do not fit the model well.[37,38] However, Voinova et al. have presented an analysis in which the soft viscoelastic film is represented by a single Voigt element and have demonstrated that their approach is able to extend beyond the Sauerbrey model.[39−42] We used both of these treatments to determine the molecular conformation of the adsorbed polymer on the surface of the substrate.

In principle, any nonionic polymer can be used to encapsulate the crystalline colloidal array (CCA). Asher et al.[7] used poly (*N*-isopropylacrylamide) (pNIPAAm) as a matrix polymer to utilize its temperature-induced volume-phase transition. This enabled the interparticle distance to be varied with temperature, such that the diffracted light was thermally tunable. This composite system can be applied to optical switching devices. In this paper, we chose this combination of the pNIPAAm matrix and the CCAs made from silica and polystyrene. The effect of the particle distribution will be separated from the effect of the particle−polymer affinity on the dynamic mechanical properties of the nanocomposite, and their relationships to the molecular structure will be discussed.

2. Materials and Methods

Materials. The synthesis of the hydrogel nanocomposites basically followed the work reported by Asher et al.[7,8,43,44] To prepare nonclose-packed colloidal crystals immobilized in a cross-linked hydrogel, an aqueous suspension containing ordered arrays of nanoparticles (silica or polystyrene) and pNIPAAm were used as the filler particle and the matrix polymer, respectively. We refer to these systems as an "ordered silica-filled hydrogel" (OSHG) or an "ordered polystyrene-filled hydrogel" (OPHG). Silica particles having diameters of 110 nm at 7.8 vol % were donated from Nippon Shokubai Co. Ltd., and polystyrene particles having diameters of 83 nm at 2.4 vol % were purchased from Polysciences Inc. These particle diameters were given from each manufacturer. Different particle concentrations were prepared either by adding deionized water, or by gradually evaporating water on a heating plate.

Both the silica and polystyrene suspensions were dialyzed against deionized water at 50 °C for three days using a pleated dialysis tubing (MWCO = 10 000, SnakeSkin, PIERCE) to obtain CCA suspensions. They were then shaken with an excess of ion-exchange resin (Bio-Rad mixed bed, AG501-X8) until an angle-dependent iridescence was observed. All the cross-linked hydrogel composites were prepared by free-radical polymerization.[18] First, NIPAAm monomer, *N*,*N*-methylenebisacrylamide (MBAAm, Sigma-Aldrich) as a cross-linker, and diethoxyacetophenone (DEAP, Sigma-Aldrich) as a light-sensitive initiator were dissolved in the CCA suspension. The monomer concentration was 1.1 M (12 wt %). Next, the solution was injected between two quartz plates separated by a 500 μm spacer and then exposed to UV light from a xenon lamp (40 mW/cm^2) for 300 s in an ice-bath. The resultant hydrogels, or the OSHG and the OPHG, were washed carefully with deionized water for 1 week.

For comparison, a conventional "hydrogel" (HG) and a "random silica-filled hydrogel" (RSHG) were also prepared at the same concentrations of each reagent. For the RSHG, the silica suspension was used as received without removing ions, such that the particles are electrostatically screened and randomly arranged. The RSHGs and OSHGs at three silica concentrations (2.6, 5.4, and 7.8 vol %) were prepared and are referred to as RSHG or OSHG followed by "−1", "−2", or "−3", respectively.

For the model study using the QCM-D, an aqueous solution of linear pNIPAAm was synthesized by UV light from NIPAAm monomer and DEAP. The resultant aqueous solution of pNIPAAm linear polymer was subsequently dialyzed with the above-mentioned dialysis tubing to remove any possible low-molecular weight contamination. The average molecular weight was determined to be $M_v = 2\,000\,000$ g/mol by a capillary viscometer.

PNIPAAm solutions at five concentrations were prepared by deionized water between c* and 0.001c*, where c* is the overlap concentration estimated as follows:

$$c^* \approx \frac{1}{[\eta]} = \frac{1}{KM_v^{\,a}} \tag{1}$$

Here $[\eta]$ is the intrinsic viscosity, M_v is the viscosity-average molecular weight, and K (=0.142) and a (=0.5) are the Mark−Houwink−Sakurada parameters.[45]

Scanning Electron Microscopy (SEM). Aqueous suspensions of silica and polystyrene nanoparticles were drop-casted on silicon wafers, and dried in vacuum overnight. The layers of dried particles were sputter-coated with Au−Pd before SEM measurements. Images were recorded using a Hitachi S-3400N scanning electron microscope with an operating voltage of 15 kV at 100 000 magnification.

Dynamic Light Scattering (DLS). Dynamic light scattering (DLS) measurements on the silica and polystyrene particles were performed using a Brookhaven Instruments Corporation (BIC) 90 Plus instrument with an incident beam of wavelength at 658 nm. The particle size distributions were calculated using Zeta Plus Particle Sizing Software Version 4.03.

Dynamic Mechanical Analysis (DMA). The shear moduli of the HG, RSHG, OSHG, and OPHG films were determined by an AR2000 Rheometer (TA Instrument) with a parallel-plate geometry. The composite samples of about 500 μm in thickness were placed on the stage and an oscillatory shear stress was applied at a constant strain amplitude of 10% to obtain the frequency dependence of tan δ. Slippage of the hydrogel relative to the bottom plate limited the possible frequency range: for the HG, the accessible range was between 0.1 and 10 Hz; for the particle-filled hydrogels, the accessible range was between 0.1 and 3 Hz, because the more elastic nature of these samples relative to the HG resulted in slippage above 3 Hz. Water was added to the samples so that they remained fully swollen during measurement.

For the stress relaxation measurement, the sample was loaded to 10% shear strain and held at that strain for 300 s at 25 °C. The reduction of the stress was continuously recorded during the relaxation period.

The viscosity of an aqueous solution of linear pNIPAAm was measured by the rheometer with a cone-and-plate geometry over the shear rate range from 10 to 500 /s.

Synchrotron Small-Angle X-ray Scattering (SAXS). SAXS experiments were performed on beamline 1−4 of the Stanford Synchrotron Radiation Laboratory (SSRL). The X-ray beam is monochromatic and has a spot size of approximately 0.25 × 1 mm^2. A two-dimensional detector was positioned at two different distances from the sample, 960 mm and 178 mm, yielding a scattering wave vector q $(=4\pi/[\lambda(\sin\theta)])$ ranging from 0.05 nm^{-1} to 12 nm^{-1}, where λ is the wavelength of the incident X-ray beam (0.149 nm) and 2θ is the scattering angle. Background and parasitic scattering were determined by separate measurements on an empty holder and subtracted. The scattering intensities were azimuthally averaged to take full advantage of the acquired data. The exposure times were 60 s for the silica-filled hydrogels (RSHG and OSHG) and 600 s for the pure hydrogel (HG) and polystyrene-filled hydrogels (RPHG and OPHG).

Quartz Crystal Microbalance with Dissipation Monitoring (QCM-D). Adsorption of pNIPAAm linear chains on silicon-dioxide-coated or polystyrene-coated quartz sensors was monitored by QCM-D. The coated quartz crystals were purchased from

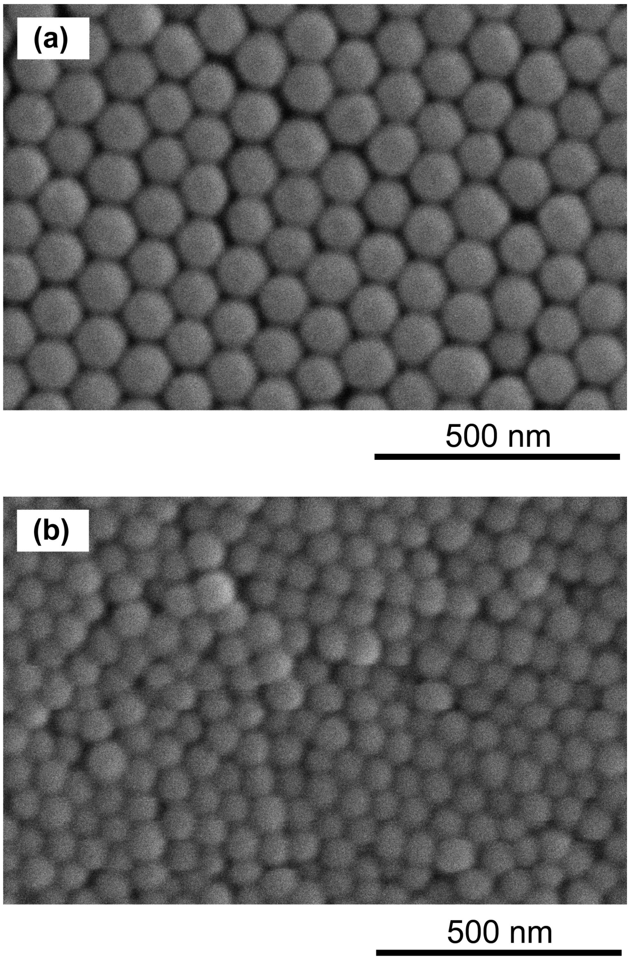

Figure 1. Scanning electron micrographs of the (a) silica and (b) polystyrene suspensions dried on silicon wafers. Note that these images do not represent the nanoparticle distribution in the hydrogel nanocomposites; the SEM images are presented simply to illustrate the particle shape and the size distribution.

Q-Sense AB (Gothenburg, Sweden), and the measurements were conducted on a Q-Sense D300 (Q-Sense AB). The QCM-D technique is based on the oscillation of a piezoelectric quartz crystal disk with a frequency (*f*) and an energy dissipation (*D*), which characterizes the mass and the viscoelastic properties of the molecules adsorbed on the crystal surface, respectively. The dissipation factor, ΔD, is defined by

$$\Delta D = \frac{E_{\mathrm{dissipated}}}{2\pi E_{\mathrm{stored}}} \tag{2}$$

where $E_{\mathrm{dissipated}}$ is the energy dissipated during one oscillation, and E_{stored} is the energy stored in the oscillating system. Before the measurement, the quartz crystals were cleaned with oxygen plasma (0.25 mbar, 6.0 W) for 5 min (with Plasma Prep5, GaLa Instrumente GmbH, Germany), rinsed with water and ethanol and dried under a stream of nitrogen gas.[42] The coated crystal was driven at its fundamental resonance frequency, f_0, of 5 MHz or at one of its first three overtones: 15, 25, or 35 MHz. To determine ΔD, the exponential decay of the oscillation amplitude was monitored after the drive circuit was short-circuited.[46,47] Shifts in frequency Δf and in dissipation ΔD were monitored at 15 ($n = 3$), 25 ($n = 5$), and 35 ($n = 7$) MHz. After the QCM-D chamber was equilibrated in water for 10 min, linear pNIPAAm aqueous solutions at various concentrations below c^* were injected into the chamber. After a 170 min adsorption period, the chamber was rinsed with water. All measurements were conducted at 25.4 ± 0.3 °C.

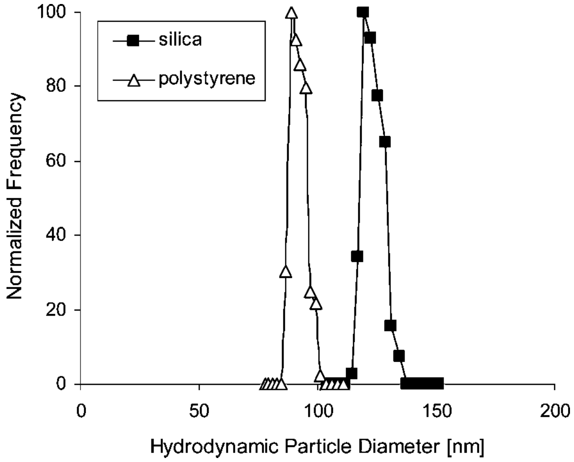

Figure 2. Hydrodynamic particle size distribution of the (a) silica and (b) polystyrene particles obtained by DLS.

3. Results

3.1. Morphology of the Nanocomposite. Particle agglomeration in the matrix polymer leads to a drastic change in the mechanical properties of nanocomposites. However, formation of an ordered colloidal array of charged nanoparticles prevents agglomeration. The spherical shape and the uniform size of the particles are the prerequisites for the formation of a crystalline colloidal structure, and SEM images were taken for the silica and polystyrene particles that were obtained by drying the aqueous suspensions. As shown in Figure 1, we can observe that both of the particles have spherical shapes and uniform sizes, and the requirements for the formation of the ordered structure were confirmed. Note that the particle alignment in these SEM images does not represent the particle distribution in the random or the ordered particle-filled hydrogel systems. This is because the interactions among the particles themselves and between the particles and the underlying silicon wafer during the drying process overrides the colloidal forces among the particles that determine the particle distribution in the suspensions and the hydrogel.

The uniform particle size was also confirmed from a sharp particle size distribution obtained by DLS, as shown in Figure 2. The particle diameters at the greatest frequency were 120 and 89 nm for silica and polystyrene particles, respectively, and were about 10% higher than the size obtained by SEM. This tendency of slightly higher particle size from DLS than that of SEM has been observed previously by several researchers;[32,48] possibly the particles drag some extra liquid along with them, for instance due to interactions with counterions in solution, giving hydrodynamic particle diameter for the DLS measurement.

A UV−vis spectrophotometer was then utilized to determine the interparticle distance within the ordered arrays that were encapsulated in the hydrogel matrix. The diffraction characteristics are given by Bragg's diffraction equation:[7,49,50]

$$\lambda_{peak} = 2 d_{hkl} n_{eff} \sin\theta \tag{3}$$

where λ_{peak} is the wavelength of the diffraction peak, d_{hkl} is the spacing between a family of lattice planes (*hkl*) (where *h*, *k*, and *l* are the Miller indices), n_{eff} is the mean effective refractive index of the sample, and θ is the angle between the incident light and the diffraction planes. In this experimental setup where light was directed normal to the sample surface, θ was $\pi/2$. The refractive indices of water, silica, and polystyrene at each wavelength were obtained using the Cauchy equation.[14,51] The composites' refractive indices were estimated as the volume-

(a) ordered silica-suspension (before network polymerization)

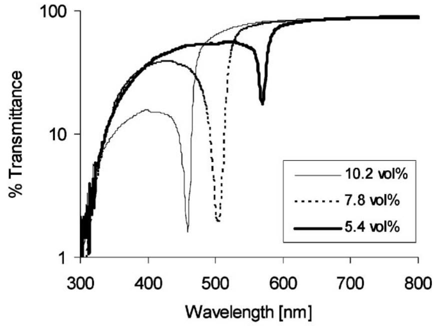

(b) ordered silica-filled hydrogel (after network polymerization)

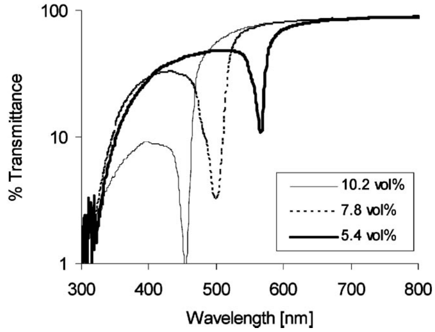

Figure 3. UV−vis extinction spectra of (a) the ordered silica-suspension before polymerization and (b) the ordered silica-filled hydrogel (OSHG) network at three different silica concentrations. The wavelength of the peak position corresponds to the interparticle distance in the composite through eq 5.

weighted averages of refractive index for each individual component, as is customarily done.[50]

Previously, we showed that our colloidal crystals adopt a locally body-centered-cubic (BCC) structure,[18] where the center-to-center particle separation, d, is related to the interplanar distance, d_{hkl}, via

$$d=\frac{d_{hkl}}{2}\sqrt{3(h^2+k^2+l^2)} \qquad (4)$$

When colloidal crystals are in a cell, the crystals orient with their most densely packed planes parallel to the walls of the cell. Since the light is incident perpendicular to the cell, the light travels along a {110} direction for a BCC structure, consistent with Monovoukas et al.[50] based on their Kossel diffraction patterns from polystyrene particles in a cell. Therefore, the interparticle distance, d, is larger than the interplanar distance, d_{hkl}, by a factor of $\sqrt{6}/2$ based on equation 4. Combined with equation 3, the interparticle distance, d, is directly related to λ_{peak} as follows:

$$d=\frac{\sqrt{6}}{4}\frac{\lambda_{peak}}{n_{eff}\sin\theta} \qquad (5)$$

On the other hand, the interparticle distance is separately given by the atomic packing factor (APF) of the BCC structure as

$$\varphi\left(\frac{d_{\text{APF}}}{D_p}\right)=0.68 \qquad (6)$$

where ϕ is the volume fraction of the particles in the system, D_{p} is the particle diameter, d_{APF} is the interparticle distance given by the APF, and the value 0.68 is the APF of the BCC structure.[50]

Figure 3 shows the UV−vis extinction spectra of the ordered silica-suspension (Figure 3a) and the ordered silica-filled hydrogel (OSHG) network (Figure 3b), where the silica concentrations are 5.4, 7.8, and 10.2 vol %. The sharp minimum in transmittance represents the diffraction from the crystalline structure formed in the ordered suspension and the cross-linked hydrogel. The interparticle distances, d, before and after the network polymerization are determined from the wavelengths of these sharp peaks at each concentration using equation 5 and are compared to d_{APF} in Table 1. The peak position blue-shifts as the silica concentration increases, which is caused by a reduction in the interparticle distance. As described earlier by Asher et al.,[6] the interparticle distance in the suspension does not change even after the polymerization of the surrounding matrix polymer. This was also confirmed with our nanocomposites by a negligible change of λ_{peak} and d upon polymerization at each particle concentration. It is important to point out that the expected interparticle distance from the volume fraction and the particle diameter d_{APF} is in close agreement with the measured d. This indicates that the particle distribution in the OSHG is uniform and homogeneous.

Table 1. Wavelength of the Diffraction Peak λ_{peak} and the Corresponding Interparticle Distance d Before and After Network Polymerization

sample silica	*a*	*b*	*a*	*b*	*a*	*b*
concentration (vol %)	5.4	5.4	7.8	7.8	10.2	10.2
λ_{peak} (nm)	568	565	503	498	458	453
n_{eff} (-)	1.341	1.341	1.347	1.347	1.352	1.353
d^c (nm)	259	258	229	226	207	205
$d_{APF}{}^d$ (nm)	256		226		207	

[a] Ordered silica-suspension (before network polymerization). [b] Ordered silica-filled hydrogel (after network polymerization). [c] Calculated from eq 5. [d] Calculated from eq 6.

In our previous report, we demonstrated that the interparticle distance was determined from the interaction potential around the particles as calculated by the DLVO theory.[18] The ζ potential of the particles and the concentration of the ionic species in the bulk solution affected the shape of the interaction potential and, hence, the interparticle distances, which were consistent with the Bragg diffraction study. In this way, the surface charge of the particles determines the interparticle distance, but does not affect the adsorption of pNIPAAm, since pNIPAAm is neutral in charge.

Note that random particle-filled hydrogels do not exhibit such a sharp extinction in UV−vis spectra (data not shown). This sharp extinction results from Bragg diffraction due to quasi-ordered structure of particles in suspensions or hydrogels; therefore, the determination of interparticle distances with this method is only possible for the ordered system.

3.2. Effect of Particle Distribution. Before we examine the interfacial affinity between the particles and the matrix polymer, the influence of the particle distribution on mechanical properties will be studied. We focus on shear stress and loss modulus properties at relatively small strain (10%), since these are sensitive to molecular interactions.

Stress Relaxation. Stress relaxation in nanocomposites should occur by one or more of the following modes: (a) between polymer chains, i.e., polymer−polymer interaction, (b) at the particle−polymer interface through adsorption and desorption of polymer chains at the particles, i.e., polymer−particle interaction, or (c) due to the particle dispersion, i.e., particle−particle interaction. To describe the stress relaxation behavior of such nanocomposites, it is common to use multiple Maxwell elements connected in parallel, with each element accounting for one

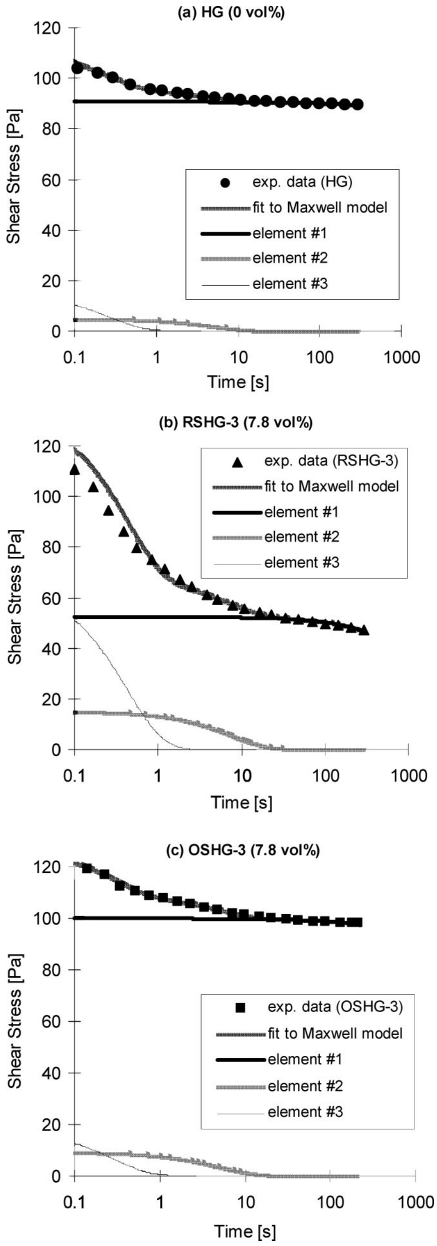
(a) HG (0 vol%)

(b) RSHG-3 (7.8 vol%)

(c) OSHG-3 (7.8 vol%)

Figure 4. Stress relaxation curves for (a) HG, (b) RSHG-3, and (c) OSHG-3. Experimental data are fitted by three Maxwell elements connected in parallel. The silica concentrations in RSHG-3 and OSHG-3 are 7.8 vol %.

relaxation mode.[52,53] In this model, the stress of each element is additive, and the overall stress is described as,

$$\sigma(t) = \sum_{i=1}^{n} \varepsilon E_i \exp\left(-\frac{E_i}{\eta_i}t\right) \tag{7}$$

where σ is the stress, ϵ is the constant strain, t is the time, and E_i and η_i are the Young's modulus and the viscosity coefficient of the ith Maxwell element, respectively. The stress relaxation curves of the HG, RSHG, and OSHG are shown in Figure 4.

All the samples that we tested showed behavior typical for an amorphous polymer. The shear stress gradually decreased over time as a result of stress relaxation. We used the commercial program OriginPro 8 to fit our experimental data. Since using only two Maxwell elements ($n = 2$) resulted in poor fitting with correlation factors (R^2) less than 0.85, we used three Maxwell elements ($n = 3$). This is reasonable given the discussion above on relaxation in the nanocomposites, and it fit the data well with correlation factors greater than 0.99. In Figure 4, three decomposed stress relaxation curves and a combined fit curve for each set of data are shown in addition to the experimental data. Of the decomposed stress relaxation curves, those with the longest, intermediate, and shortest relaxation times are referred to as Maxwell elements #1, #2, and #3, respectively. We attribute each Maxwell element to a distinct relaxation process that takes place in the nanocomposite, and their physical interpretation will be discussed in detail in the Discussion section. As is apparent in Figure 4, the relative reduction of the stress after 100 s is much larger for RSHG than HG and OSHG. Since the major difference among the three nanocomposites is the presence of silica particles and their distribution, these factors must explain the observed differences.

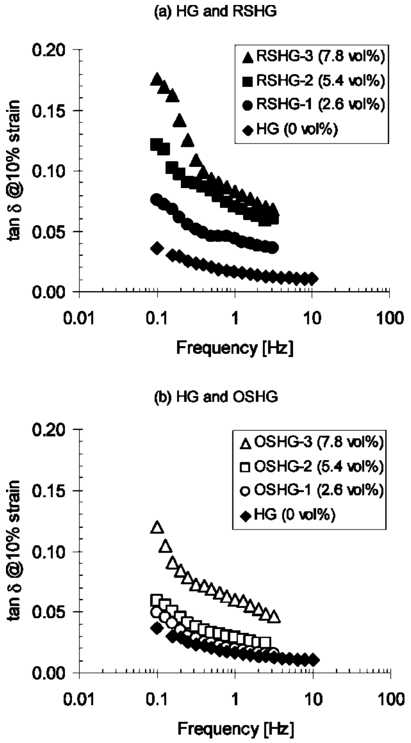
(a) HG and RSHG

(b) HG and OSHG

Figure 5. Tan δ as a function of frequency for (a) HG/RSHG and (b) HG/OSHG. Silica concentrations are indicated in parentheses in the inset.

Viscoelastic Loss Properties by DMA. Dynamic mechanical analysis is a powerful method to investigate the properties of viscoelastic materials. When mechanical strain is applied to a viscoelastic material, the resultant stress is delayed by a phase lag, δ, which depends on the energy dissipation due to internal molecular motion. Let the applied strain and the resultant stress amplitudes be γ_0 and σ_0, respectively. Then, the complex shear modulus, G^*, of the nanocomposites is defined by

$$G^* = \left(\frac{\sigma_0}{\gamma_0}\right)\cos\delta + i\left(\frac{\sigma_0}{\gamma_0}\right)\sin\delta = G' + iG'' \tag{8}$$

where G' is the storage modulus and G'' is the loss modulus. The ratio of G'' to G', or tan δ, is a measure of energy dissipation within the material, and its determination allows us to investigate the internal molecular motion.[54]

We applied a constant shear strain amplitude of 10% to our nanocomposites as a function of the oscillation frequency. The resultant stress and the phase lag were monitored by the rheometer. To determine the effect of particle agglomeration and concentration, three RSHGs and OSHGs with silica concentrations of 2.6, 5.4, and 7.8 vol % were measured. The frequency dependence of tan δ is shown in Figure 5, where different silica concentrations and distributions are compared.

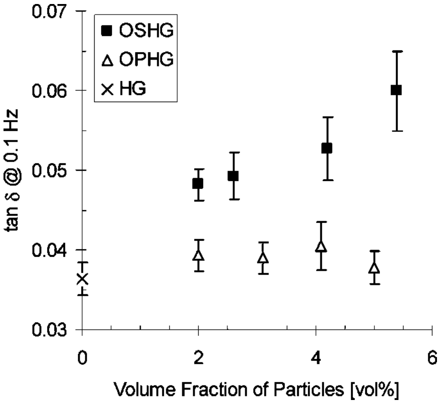

Figure 6. Viscoelastic loss, tan δ, at 0.1 Hz of HG, OSHG, and OPHG as a function of the particle concentration.

HG demonstrates a typical viscoelastic behavior within the frequency range, showing gradual reduction in tan δ as the frequency increases. This is explained by the inability of the polymer to follow the oscillating plate at higher frequency. Tan δ is higher for RSHG than HG at all frequencies over the entire concentration range. This must be due to the agglomeration of silica particles and from a particular molecular interaction of the adsorbed polymer on the silica particles. The detailed molecular conformation of the adsorbed polymer, comparing silica and polystyrene surfaces, will be investigated in section 3.4. Moreover, tan δ for OSHG is significantly lower than that for RSHG at all concentrations. Because the particle agglomeration in OSHG is much smaller than RSHG, this smaller tan δ for OSHG than for RSHG must be caused by the reduced amount of the agglomerated particles.

3.3. Effect of Particle−Polymer Affinity. We now investigate how much the particle−polymer affinity affects the mechanical properties when we eliminate particle agglomeration. Increasing the particle concentration within the ordered particle-filled hydrogels does not increase the particle agglomeration, but the interparticle distance is decreased, maintaining the locally ordered structure of particles (Figure 3). In this system, we should be able to eliminate the effect of particle agglomeration and to determine the effect of the particle-matrix affinity. We focused on tan δ of the nanocomposite, since this probes the internal molecular motion within the system. As shown in Figure 5, tan δ is a function of frequency. We picked a single value of tan δ at 0.1 Hz to represent the magnitude of energy dissipation of the material, because no cross-over was observed among tan δ curves within the frequency range in Figure 5.

Tan δ at 0.1 Hz is plotted against the particle concentration for the ordered particle-filled hydrogels in which silica (OSHG) and polystyrene (OPHG) were incorporated without agglomeration (Figure 6). The highest concentration achieved without agglomeration for polystyrene was only 5 vol %, because polystyrene particles tend to agglomerate in aqueous systems more easily than silica particles due to their hydrophobicity. For OSHG, tan δ monotonically increased as the particle concentration increased. Because there is essentially no particle agglomeration in these ordered composites, this increase in tan δ is simply caused by the increased contact area between the particle and the matrix polymer, where physical adsorption and desorption of the polymer chains take place on the surface of silica particles. However, the behavior of tan δ with particle concentration is different with OPHG; in contrast to OSHG, tan δ remains at nearly the same value as for the HG. This difference of tan δ behavior can only result from the way the polymer interacts with the surfaces of the silica and polystyrene. In the following sections, we present a detailed investigation of the interfacial layer between the particles and the polymeric matrix using synchrotron SAXS and QCM-D to clarify the molecular conformation of the polymer.

3.4. Analysis of the Interfacial Diffuse Layer. *3.4.1. Synchrotron Small-Angle X-ray Scattering (SAXS).* According to Porod's Law,[55] the SAXS intensity for spherical particles, $I(q)$, should decrease as q^{-4} for large q, with the proportionality constant related to the total area S of the boundaries between the two phases as,

$$I(q) \xrightarrow[q\to\infty]{} \frac{2\pi(\Delta\rho)^2 S}{q^4} \tag{9}$$

where $\Delta\rho$ is the difference in electron density of the two phases. However, Porod's Law is only valid for the ideal two-phase system defined as follows: (1) The system contains only two distinct regions, and (2) the boundary between these two regions is sharp without any measurable thicknesses. A real material never satisfies these ideal conditions, and two types of deviations from Porod's Law have been observed.[34]

A positive deviation is caused by the background scattering from the pure individual phases. To correct for this, we measured the scattering intensity of the pure hydrogel (HG) without nanoparticles, and subtracted it from the net observed intensity of the particle-filled hydrogels.

By contrast, a negative deviation is related to the existence of a diffuse transition region between two phases. In our case, the roughness of the particle surface gives rise to this transition zone; a perfectly smooth surface would not have this region. The scattering length density distribution in a two-phase material with diffuse boundaries, $\rho(r)$, is described by

$$\rho(r) = \rho_{id}(r) \times g(r) \tag{10}$$

where $\rho_{\mathrm{id}}(r)$ is the density distribution in the hypothetical system in which all the diffuse boundaries have been replaced by sharp boundaries, and $g(r)$ is a smoothing function characterizing the diffuse boundary. If the electron density decreases in sigmoidal shape within the phase boundary, $g(r)$ can be approximated well by a Gaussian function:

$$g(r) = \left(\frac{1}{\sqrt{2\pi}\sigma}\right) \exp\left(\frac{-r^2}{2\sigma^2}\right) \tag{11}$$

Here σ is related to the thickness, t, of the transition zone as[34]

$$t = \sqrt{2\pi}\sigma \tag{12}$$

The scattering intensity of SAXS is given by the absolute square of the Fourier transform of $\rho(r)$, that is, by

$$I(q) = I_{id}(q)G^2(q) \tag{13}$$

$$G(q) = \exp(-(\sigma^2/2)q^2) \tag{14}$$

where $G(q)$ is the Fourier transform of $g(r)$. For small σ ($\sigma q \ll 1$), eq 13 can be approximated by

$$I(q) = I_{id}(q)(1 - \sigma^2 q^2) \tag{15}$$

Substituting eq 15 into eq 9 yields

$$I(q)q^4 = \lim_{q\to\infty}[K_p(\Delta\rho)^2 S - \{K_p(\Delta\rho)^2 S\cdot\sigma^2\}q^2] \tag{16}$$

where K_{p} is a proportionality constant.

Equation 16 indicates that a plot of $I(q)q^4$ against q^2 should give a linear relationship with its y-intercept equal to $K_{\mathrm{p}}(\Delta\rho)^2S$ and its slope equal to $-K_{\mathrm{p}}(\Delta\rho)^2S\sigma^2$ at large q, thus permitting the evaluation of σ and t.

Following the above procedure, we determined the thickness of the diffuse layer for silica-filled and polystyrene-filled hydrogels. The raw scattering intensities of OSHG and OPHG are shown in Figure 7. A strong positive deviation from Porod's

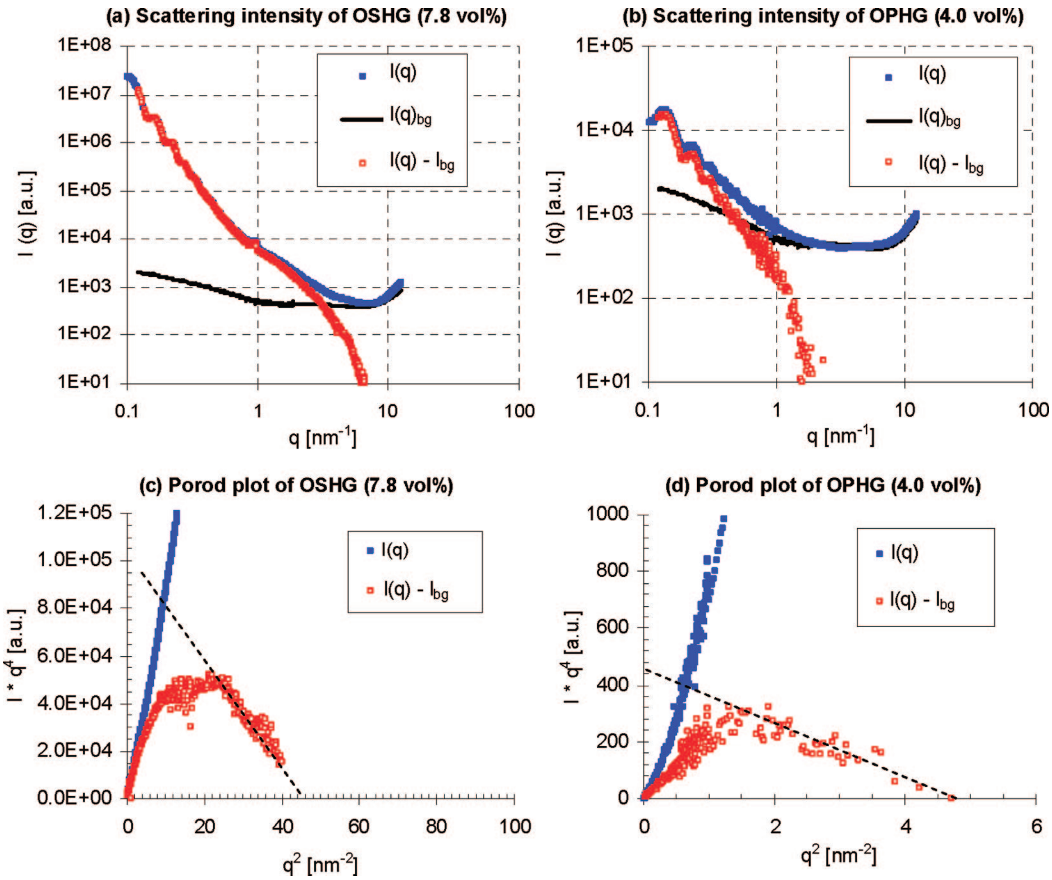

Figure 7. Scattering intensities $I(q)$ of (a) ordered silica-filled hydrogel (OSHG) and (b) ordered polystyrene-filled hydrogel (OPHG). Background intensity $I(q)_{bg}$ is obtained by measuring the pure hydrogel (HG), and is subtracted from each scattering intensity of the nanocomposites. Porod plots of (c) OSHG and (d) OPHG. Dashed lines are drawn to obtain the thickness of the diffuse layer on the particles using eq 16.

Table 2. Thickness of the Diffuse Interfacial Layer for Particle-filled Hydrogels Determined by Synchrotron SAXS

particle	silica	silica	silica	silica	silica	silica	polystyrene	polystyrene	polystyrene	polystyrene
particle distribution	random	ordered	random	ordered	random	ordered	random	ordered	random	ordered
particle concentration (vol %)	2.6	2.6	5.4	5.4	7.8	7.8	3.0	3.0	4.0	4.0
diffuse layer thickness (nm)	0.34	0.29	0.29	0.32	0.35	0.30	1.12	1.11	1.15	1.12

Law at high q range was observed for both cases. This influence of the background scattering from the polymer can be removed by subtracting the scattering intensity of the pure hydrogels, $I(q)_{bg}$ (Figure 7, parts a and b). Here, the unit of the scattering intensity is arbitrary, and the measured curves were vertically shifted such that their intensities in the positive deviation region superimpose onto each other. This accounts for any nonuniformity and the different hydrogel concentrations in the different samples. After the background was subtracted, a negative deviation from Porod's Law appeared. To extract the thickness of the diffuse layer using eq 16, we plotted the background subtracted intensity, $I - I_{bg}$, against q^2 (Figure 7, parts c and d). As q^2 increased from 0 to about 20 nm^{-2} for OSHG, and from 0 to about 2 nm^{-2} for OPHG, $q^4I(q)$ increased (most likely due to an imperfect background subtraction), approached an approximately constant value, then decreased at higher q. From the linear relationship in this high q range (ie. $q^2 > 20$ nm^{-2} for OSHG and $q^2 > 2$ nm^{-2} for OPHG), the thicknesses of the diffuse interfacial layer t were determined as 0.35 and 1.12 nm for OSHG and OPHG, respectively. Although there is some ambiguity in the range of q^2 to use in the determination of t, the difference of these two materials is much larger than this experimental error; note the large difference in the x-axis scale between parts c and d of Figure 7.

In Table 2, the thicknesses of the diffuse layers obtained from the SAXS measurements are summarized at various particle distributions and concentrations. The surface roughness of the silica particles in the hydrogel is only a few angstroms, but the polystyrene particles are much rougher than the silica particles. The surface roughness determined by this method does not depend on either the particle distribution or the concentration, but only on the particle species. This is because the q range used for obtaining the thickness of the interfacial layers is completely different from that for the particle size. The q range for the interfacial layer is above 1 nm^{-1}, and the corresponding length scale is too small to observe the particle size distribution. Therefore, the surface roughness that is independent of the particle size distribution or the concentration is expected and the consistency supports our analysis.

Note that a perfect crystalline material would show Bragg diffraction peaks in the SAXS data, which correspond to higher order diffraction described in eq 4. In parts a and b of Figure 7, however, such diffraction peaks are not observed. This indicates that the array of particles has only short-range or local order in our nanocomposites and is consistent with the UV−vis diffraction peaks that have a finite value of half-width (Figure 3).

3.4.2. Quartz Crystal Microbalance with Dissipation Monitoring (QCM-D). Adsorption behavior of linear pNIPAAm and the viscoelastic properties of the adsorbed layer were studied using quartz crystals coated with silicon dioxide (silica) and polystyrene to obtain more information on the interfacial layer.

(a) Adsorption on Silicon Dioxide Surface

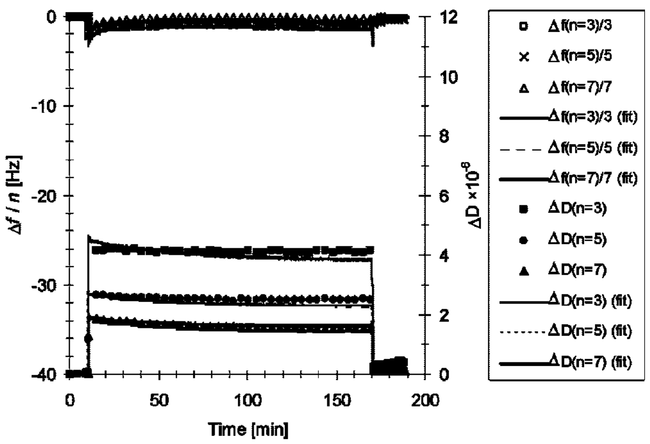

(b) Adsorption on Polystyrene Surface

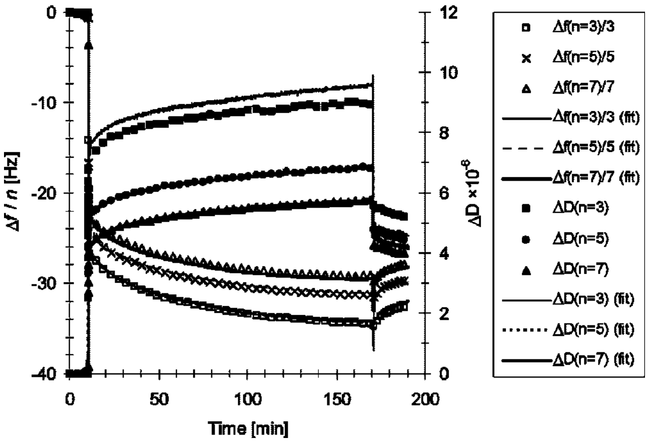

Figure 8. QCM-D data of pNIPAAm solution adsorbed on the (a) silicon dioxide and (b) polystyrene surfaces. At 10 min, the pNIPAAm solution at the overlap concentration c^* is injected into the QCM-D chamber, and at 170 min, water was injected to rinse the adsorbed polymer on the substrate. The experimental data are fitted to the Voigt−Voinova model.

If the adsorbed material is evenly distributed, rigidly attached, and thin (i.e., the film mass is small compared to the mass of crystal), the frequency shift $\Delta f = f - f_0$ is related to the adsorbed mass per unit surface, Δm, by the Sauerbrey equation:[36]

$$\Delta m = -\frac{C \cdot \Delta f}{n} \tag{17}$$

where C is the sensitivity constant of the quartz crystal (17.7 ng Hz^{-1} cm^{-2}) and n is the harmonic number.

In Figure 8, Δf values normalized by n and dissipation factor ΔD (the ratio of the energy dissipated during one oscillation to the energy stored in the oscillation system (see equation 2) measured at 15, 25, and 35 MHz, are plotted as a function of time for pNIPAAm aqueous solution at overlap concentration c^* (see eq 1) on silicon dioxide and polystyrene. In spite of the identical concentration of pNIPAAm solution, the magnitude of Δf for polystyrene is much larger than Δf for silicon dioxide. The normalized Δf values do not superimpose onto one another, especially for polystyrene, which means that the adsorbed layer on polystyrene is viscoelastic and does not satisfy the required condition for the Sauerbrey equation (eq 17).

After the adsorption equilibrium was reached, water was injected at 170 min to rinse the adsorbed polymer from the substrate. From the change of Δf and ΔD after 170 min, there is a clear difference in the polymer desorption between silicon dioxide and polystyrene. The adsorbed polymer on silicon dioxide desorbed almost completely immediately after this rinse, but the adsorbed layer on polystyrene did not wash off completely. This shows that the polymer layer adsorbs more strongly on polystyrene than on silicon dioxide.

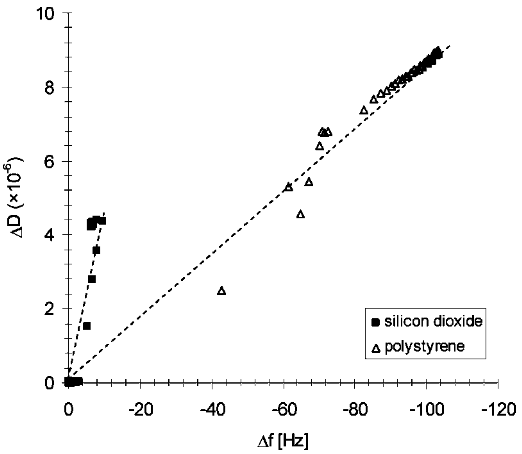

Figure 9. Change in the dissipation factor ΔD as a function of the change in frequency Δf for the adsorption of pNIPAAm solution at the overlap concentration c^* onto silicon dioxide and polystyrene surfaces. $f_0 = 5$ MHz, $n = 3$.

In Figure 9, we replotted the QCM-D results as the change in energy dissipation ΔD versus the frequency change Δf. This plot is frequently used to investigate conformation and viscoelasticity of the adsorbed layers as a first approximation, although Δf is not exactly proportional to the adsorbed mass.[38,56] A linear relation is found for both of the surfaces, and the slope of the line is higher for silicon dioxide. This indicates that the adsorbed layer on silicon dioxide shows larger energy dissipation per adsorbed mass, and is thus "softer" than the adsorbed layer on polystyrene.

To extract more quantitative viscoelastic properties of the adsorbed layer, we apply the model presented by Voinova et al.[39−42] In this Voigt−Voinova model, the adsorbed film is represented by a single Voigt element, where the quartz crystal is assumed to be purely elastic, and the surrounding liquid to be purely viscous and Newtonian. The density ρ_l and viscosity η_l of the bulk liquid are assumed to be those of water. This is a valid assumption for the density, because the density of the pNIPAAm (0.9 g/cm^3) is close to that of water. The other assumption of the viscosity will be verified below. Further, it is assumed for simplicity and to achieve a tractable analysis that the thickness t_f and the density ρ_f of the adsorbed film are uniform, that the viscoelastic properties are frequency independent, and that there is no slip between the adsorbed layer and the crystal during shear.[39]

Rodahl et al. showed that Δf and ΔD are given by the imaginary and real parts of the β-function, respectively:[57]

$$\Delta f = \mathrm{Im}\left(\frac{\beta}{2\pi\rho_q t_q}\right) \tag{18}$$

$$\Delta D = -\mathrm{Re}\left(\frac{\beta}{2\pi\rho_q t_q}\right) \tag{19}$$

$$\beta = \xi_1 \frac{2\pi f \eta_f - i\mu_f}{2\pi f} \frac{1 - \alpha\exp(2\xi_1 t_f)}{1 + \alpha\exp(2\xi_1 t_f)} \tag{20}$$

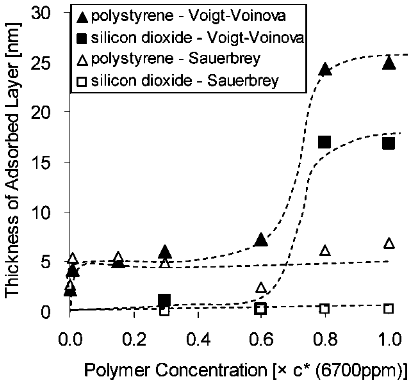

Figure 10. Thickness of the adsorbed layer on the polystyrene and silicon dioxide surfaces at various pNIPAAm concentrations. Open symbols are based on calculation from the Sauerbrey model, and closed symbols are from the Voigt−Voinova model. Dashed lines are to guide the eye.

$$\alpha=\frac{\frac{\xi_1}{\xi_2}\frac{2\pi f\eta_f-i\mu_f}{2\pi f\eta_l}+1}{\frac{\xi_1}{\xi_2}\frac{2\pi f\eta_f-i\mu_f}{2\pi f\eta_l}-1},\qquad \xi_1=\sqrt{-\frac{(2\pi f)^2\rho_f}{\mu_f+i2\pi f\eta_f}},$$

$$\xi_2=\sqrt{i\frac{2\pi f\rho_l}{\eta_l}} \tag{21}$$

where ρ is the density, t is the thickness, μ is the storage modulus, η is the loss modulus, and f is the measured frequency. The indexes q, f, and l refer to the quartz crystal, adsorbed film, and bulk liquid, respectively. Since the adsorbed layer is viscoelastic, we can also define the mechanical loss tangent, tan δ_f, as

$$\tan\delta_f=\frac{2\pi f\eta_f}{\mu_f} \tag{22}$$

Results from measurements at three overtones (Figure 8) were fitted to the Voigt−Voinova model. The density ρ_f, the thickness t_f, the viscosity η_f, and the shear modulus μ_f of the adsorbed film were adjusted to give the best possible fit using the commercial program Q-Tools from Q-Sense AB. Because we are interested in the state of adsorption at equilibrium, Δf and ΔD values were averaged over the last 10 min before the rinse and were used in the fitting calculation.

We varied the pNIPAAm concentrations and conducted adsorption experiments to obtain adsorption isotherms. The thickness of the adsorbed layer was calculated at different polymer concentrations by both the Sauerbrey and the Voigt−Voinova models, and is shown in Figure 10.

For adsorption on polystyrene below 0.3c*, the thickness of the adsorbed film is well-described by both the Sauerbrey and the Voigt−Voinova models. This indicates the film is rigid. Above 0.3c*, the Sauerbrey thickness underestimates the Voigt thickness since the layer is viscoelastic. For adsorption on silicon dioxide, on the other hand, there is essentially no observable adsorption below 0.5c*. At the overlap concentration c* of pNIPAAm, an adsorbed layer of about 17 nm thick was observed based on the Voigt−Voinova model. But the important point is that, for the entire pNIPAAm concentration including c*, the layer thickness on the silicon dioxide is smaller than the thickness on the polystyrene surface.

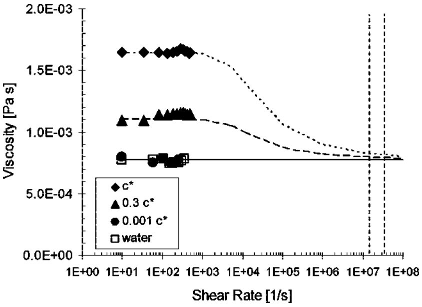

Figure 11. The viscosity of water and pNIPAAm solutions (0.001c*, 0.3c*, and c*) as a function of the shear rate. Experimental data are limited to the shear rate up to 500 [1/s], and the anticipated shear-thinning behavior is obtained from the fitting to eq 23. The two vertical dotted lines indicate the operating frequencies of the QCM-D.

We assumed that the viscosity of the bulk liquid η_l is identical to that of water. To verify this assumption, the viscosity of the pNIPAAm solution was measured by the rheometer at shear rates between 10 and 500 [1/s]. Many aqueous polymer solutions show shear-thinning behavior, and, therefore, it is likely that the viscosities measured at these low shear rates do not represent the viscosity of the fluid monitored by the QCM-D because it operates at a much higher frequency. To describe the shear-thinning behavior of the polymer solution, Munro et al. [42] used the Carreau model:

$$\eta(\dot{\gamma})=\eta_\infty+\frac{\eta_0-\eta_\infty}{[1+(\tau\dot{\gamma})^2]^{p/2}} \tag{23}$$

where $\dot{\gamma}$ is the shear rate, η_∞ is the viscosity at infinite shear rate (estimated as a viscosity of water), η_0 is the zero-shear viscosity, τ is a fitting parameter that describes the characteristic time scale, and p is a fitting parameter that describes how quickly the viscosity decreases.[58] The characteristic time, τ, can be estimated from the Rouse model, which gives the longest relaxation time, τ_1:

$$\tau_1=0.608\frac{(\eta_0-\eta_\infty)M_{\rm w}}{cRT} \tag{24}$$

where c is the mass concentration of the polymer solution, R is the gas constant, and T is the temperature. Vlassopoulos et al.[59] studied the shear-thinning behavior of polyacrylamide solutions and found that τ is larger than τ_1 by a factor of about three. We use this relationship for our pNIPAAm solutions since the chemical structure of the polymer is similar to their polyacrylamide.

The shear-thinning behavior of the pNIPAAm solutions is shown in Figure 11, along with the fitting curves to eq 23. The characteristic times of the quartz oscillation, taken as the inverse of the operating frequency at 15 and 35 MHz, are shown as vertical lines. It is clear that all of our pNIPAAm solutions are almost completely shear-thinned at the operating frequency of the QCM-D. Thus, the assumption of the identical viscosity of the bulk liquid to that of water has been verified.

The viscoelastic parameters obtained from the QCM-D are summarized in Table 3. At pNIPAAm concentration of 0.001c*, tan δ_f of the layer adsorbed on the polystyrene is smaller than unity: the energy dissipation is small and the polymer layer is considered to be rigid. At higher polymer concentrations above 0.3c* for both silica and polystyrene, tan δ_f is greater than unity, suggesting a formation of soft layers, and a deviation between the Voigt−Voinova thickness and the Sauerbrey thickness was observed.

4. Discussion

4.1. Effect of Particle Distribution. *Stress Relaxation.* From Figure 4, one can see that the stress relaxation curve of HG is dominated by Maxwell element #1, and that the contributions from elements #2 and #3 are small and almost negligible. Considering that HG consists only of polymer, the relaxation process with the longest relaxation time corresponds to the

Table 3. Summary of the Physical Properties of the Adsorbed Layer on Silicon Dioxide and on Polystyrene

adsorbent			unit	silicon dioxide				polystyrene			
pNIPAAm concentration			c^*	0.001−0.15	0.30	0.80	1.00	0.001	0.30	0.80	1.00
			ppm	10 ~ 1000[a]	2000	5360	6700	10	2000	5360	6700
Sauerbrey model	thickness	$t_{n=3}$	nm	-	0.0	0.2	0.3	2.7	4.9	6.2	6.8
	frequency shift	$\Delta f_{n=3}/3$	Hz	-	−0.1	−1.1	−1.3	−13.8	−24.6	−31.2	−34.4
		$\Delta f_{n=5}/5$	Hz	-	−0.2	−1.2	−1.1	−13.2	−22.5	−28.5	−31.3
		$\Delta f_{n=7}/7$	Hz	-	0.0	−0.3	−0.2	−12.9	−21.3	−26.7	−29.2
	dissipation shift	$\Delta D_{n=3}$	10^{-6}	-	1.1	3.5	3.9	0.9	4.2	7.2	9.0
		$\Delta D_{n=5}$	10^{-6}	-	0.7	2.1	2.3	0.8	3.5	5.1	6.8
		$\Delta D_{n=7}$	10^{-6}	-	0.5	1.5	1.6	0.7	2.9	4.5	5.7
Voigt -Voinova model	thickness: t_f		nm	-	1.1	17.0	16.9	2.2	6.1	24.3	25.0
	density: ρ_f		kg/m^3	-	3000	2684	2926	827	1411	2113	2143
	viscosity: η_f		kg/ms	-	3.0E−04	3.2E−04	3.1E−04	4.4E−03	9.7E−04	5.7E−04	5.7E−04
	shear modulus: μ_f		Pa	-	4.2E+03	5.0E+03	4.5E+03	1.2E+06	2.4E+04	1.2E+04	9.9E+03
	tan δ_f @15 MHz ($n = 3$)			-	6.7	6.0	6.6	0.4	3.8	4.6	5.5

[a] Polymer adsorption was not observed at the low pNIPAAm concentrations.

Table 4. Relative Importance of Each Maxwell Element and Fitting Parameters in Equation 7

sample name	HG	RSHG-1	RSHG-2	RSHG-3	OSHG-3
silica distribution	-	random	random	random	ordered
silica concentration (vol %)	0.0	2.6	5.4	7.8	7.8
relative importance of #1 C_1	0.93	0.87	0.58	0.40	0.79
elasticity coefficient E_1 (Pa)	840	1298	692	523	998
viscosity coefficient η_1 (Pa s)	5.1E+07	4.3E+07	2.8E+06	1.3E+06	8.9E+06
relaxation time τ_1 (s)	6.0E+04	3.3E+04	4.0E+03	2.5E+03	8.9E+03
relative importance of #2 C_2	0.02	0.03	0.13	0.11	0.07
elasticity coefficient E_2 (Pa)	14	52	155	150	92
viscosity coefficient η_2 (Pa s)	353	576	1305	1108	463
relaxation time τ_2 (s)	25	11	8	7	5
relative importance of #3 C_3	0.05	0.10	0.29	0.49	0.14
elasticity coefficient E_3 (Pa)	46	150	343	647	180
viscosity coefficient η_3 (Pa s)	78	129	225	274	51
relaxation time τ_3 (s)	1.7	0.9	0.7	0.4	0.3

polymer−polymer interaction. We define the relative importance of the *i*-th element with respect to the whole system C_i, focusing on the coefficient of each term in equation 7 as,

$$C_i = \frac{E_i}{E_1 + E_2 + E_3}, \qquad (i = 1, 2, 3) \tag{25}$$

The fitting parameters in eq 7 of the composite samples and the relative importance C_i are summarized in Table 4.

We measured the relaxation behavior of the RSHG at three different particle concentrations. RSHG-1, RSHG-2 and RSHG-3 are different only in the particle concentrations (2.6%, 5.4% and 7.8%, respectively). C_i values for the three RSHGs are smaller than for HG due to enhanced contributions of elements #2 and #3, whose relaxation times are shorter than element #1. The higher concentration of particles resulted in much larger contribution from element #3 and, hence, a smaller contribution from element #1. Furthermore, with increased particle concentration, element #3 becomes progressively more important compared to element #1. These observations suggest that element #3 represents the relaxation process occurring from the particle−particle interactions because the higher concentration of particles in a random system has more agglomerated particles. These agglomerated particles can be dispersed when we apply shear stress, and this is a major source of the stress relaxation in RSHG.

We further examined the stress relaxation behavior of OSHG-3. The particle distribution has been proven to be uniformly ordered in OSHG-3. One can expect that the relaxation process resulting from particle−particle interaction should be smaller than RSHG-3. Compared to RSHG-3, the reduction of C_i for OSHG is indeed much larger for element #3 (0.49 to 0.14) than element #2 (0.11 to 0.07, see Table 4). This is consistent with the relaxation behavior discussed in the previous paragraph, where the higher (agglomerated) particle concentration in RSHG resulted in higher C_3. From this, we conclude that the Maxwell elements #2 and #3 correspond to the (b) particle−polymer and (c) particle−particle interactions, respectively.

Note that the reason why C_1 for HG is not 1, but 0.93, is because of the polydispersity of the hydrogel network. Even within a single hydrogel, a certain region of the network chains experience different constraint from other regions. This polydispersity resulted in finite numbers of relaxation processes in the sample. In our analysis, HG happens to show three relaxation modes, but this number is arbitrary, depending on how we split the relaxation curve in Figure 4a. Compared to having nanoparticles that lead to much larger additional relaxation process, however, HG is mostly dominated by a single relaxation mode.

Shear Modulus of Nanocomposites. In Figure 5, we demonstrated that changing the particle distribution (RSHG and OSHG) resulted in a significant change in tan δ of the nanocomposite. The process of the energy dissipation is strongly related to that of the stress relaxation. It is quite natural to consider that the energy dissipation takes place through the same interactions as the stress relaxation, that is, (a) polymer−polymer, (b) particle−polymer, and (c) particle−particle interactions. In RSHGs, the higher silica concentration resulted in higher tan δ, since these nanocomposites have larger contributions from parts b and c. When the silica agglomeration is reduced in OSHG, tan δ decreased from that for RSHG, which is most likely explained by a reduced contribution from part c.

So far, we have demonstrated that three Maxwell elements connected in parallel are sufficient to quantitatively fit the three stress relaxation processes that occur in our particle-filled hydrogels and that the particle distribution has a significant effect on the stress relaxation behavior of the nanocomposites. Moreover, the tan δ values certainly reflect the internal microstructure of our nanocomposites and should be a suitable measure of particle−polymer affinity. In the following section, this relationship is discussed in detail.

4.2. Effect of Particle−Polymer Affinity

Since the nanocomposites shown in Figure 6 are ordered, particle-filled hydrogels, the effect of particle agglomeration is small. Therefore, the major source of the difference in tan δ is the difference in the affinity between the particle and the surrounding pNIPAAm polymer. The difference in tan δ between these two particle-filled nanocomposites is more pronounced at higher particle concentration. This is reasonable, considering that only the polymer chains adjacent to the particles give rise to this difference in viscoelasticity.

It is possible for pNIPAAm to interact both with hydrophobic and hydrophilic surfaces, since this polymer has a hydrophilic amide group and a hydrophobic isopropyl group on its side chain.[60] Physical adsorption of pNIPAAm on silica and polystyrene surfaces likely takes place via hydrogen bonds and dispersive interactions,[61] respectively. Considering the observation that incorporation of polystyrene does not increase tan δ of the nanocomposite in Figure 6, we hypothesize that the surrounding pNIPAAm chains tightly adsorb on the polystyrene surface. This limits any energy dissipation that would result through (b) particle−polymer interactions. For silica-filled hydrogels, on the other hand, although there is some interaction between silica and pNIPAAm, it is rather weaker than the one for the polystyrene system. Our hypothesis, thus, is that this weak interaction allows pNIPAAm chains in the vicinity of the silica surface to adsorb and desorb on the surface, which causes a conformational change of the chains, leading to additional energy dissipation and the resulting increase in tan δ.

To test this hypothesis, we focus on the boundary region between the particle and the matrix polymer. Recall that the surface roughness of the particles embedded in the matrix polymer was determined by synchrotron SAXS, and the viscoelastic properties of the modeled systems were measured using QCM-D showing the detailed molecular conformation of the adsorbed layer.

The synchrotron SAXS study revealed that the surface roughness of the silica particles is smaller (~0.3 nm) than the length of the Kuhn monomer of the polymer chain (~1 nm). The Kuhn length is a statistical length scale with which the polymer chain undergoes a random walk in a Θ condition.[62] Since the polymer chain cannot "see" roughness smaller than its Kuhn length, the silica surface appears flat to the polymer chain. On the other hand, the magnitude of the surface roughness on the polystyrene particles (~1.1 nm) is comparable to the Kuhn length, and the polymer chain is able to recognize the surface as rough on a molecular scale.

Several theoretical papers dealing with polymer adsorption on topologically modified surfaces have been published.[63−68] These articles reach the general conclusion that roughness affects adsorption, and that an enhancement of adsorption on a rough surface compared to a flat surface is to be expected in many cases. Ball et al. found that a surface that is curved, corrugated, or rough will adsorb polymer chains even when a flat surface that has the identical surface chemistry exhibits no adsorption.[65] Vilgis and Heinrich presented various models for adsorption of polymers on surfaces, which range from weak random surfaces to fractal surfaces with larger roughness.[67] They reported that, for all of their models, adsorption is enhanced on rough surfaces compared to flat surfaces. They explained this enhancement from the viewpoint of conformational entropy: when a polymer chain adsorbs on a flat surface, it needs to stretch out to gain adsorption energy, but the large conformational change of the chain carries an entropy penalty. Consequently, polymer chains that adsorb to a flat surface tend to gain little adsorption energy, and can be easily desorbed from the surface. In the case of rough surfaces, like those of our polystyrene particles, the entropy penalty of the adsorbed polymer chains is lower, and they are more strongly adsorbed on the surface. This topological effect due to the surface roughness presumably explains the strong adsorption of the polymer on the polystyrene particles, with the resulting smaller energy dissipation than on the silica particles. However, this discussion is based purely on the surface roughness, and therefore, we need more characterization from the viewpoint of the molecular interaction between the pNIPAAm chains and the particles. Such detailed information on the molecular conformations of the adsorbed polymer was obtained by the QCM-D. In these experiments, we assume that the surface of the coated quartz crystals is flat, and that the above-mentioned topological effect due to the surface roughness is negligible.

From Figure 9, a linear relationship between Δf and ΔD was observed for both substrates, with the slope being smaller for the layer on the polystyrene than on the silicon dioxide. This suggests that the energy dissipation per unit adsorbed mass of polymer chains on polystyrene is smaller than on silicon dioxide. The smaller dissipation on polystyrene is also confirmed from smaller tan δ_f (Table 3). Both of these observations indicate that the adsorbed layer is more rigid on polystyrene than on silicon dioxide. Moreover, the adsorbed masses on these two surfaces are directly compared using Δf below the pNIPAAm concentration of 0.3c*, where the Sauerbrey condition is valid (Table 3). In this regime, the adsorbed mass is proportional to Δf, according to eq 17. Δf values for the polystyrene are much larger than for the silicon dioxide, indicating the larger adsorption of the polymer on the polystyrene. All of the QCM-D data presented here indicate that more pNIPAAm chains adsorb on the polystyrene and they form more rigid layers than the polymer on the silicon dioxide.

The adsorption isotherm (Figure 10) provides us with further information on the molecular conformation of the adsorbed layer. Below the pNIPAAm concentration of 0.3c*, the pNIPAAm adsorbed only to the polystyrene surface. This indicates that the interaction between the polystyrene surface and the polymer is stronger than the silicon oxide. This stronger interaction is also confirmed from the Δf and ΔD values that showed only a partial recovery after water was injected to rinse the adsorbed polymer on the polystyrene. On the contrary, the layer on the silicon dioxide exhibited almost a complete recovery after the rinse (Figure 8). White et al. reported that adsorbed layers with ΔD exceeding a critical value (2×10^{-6}) were not applicable for analysis using the Sauerbrey equation.[69] The adsorbed layer above 0.3c* has ΔD greater than this critical value, and tan δ_f is greater than unity. Both observations indicate that the thickness of the layer should be determined by the Voigt−Voinova model.

Considering the above discussion, the adsorption process for pNIPAAm chains to the polystyrene and the silicon dioxide flat surfaces is schematically illustrated in Figure 12. At low pNIPAAm concentration below 0.3c*, pNIPAAm adsorbs onto polystyrene with a flat conformation via dispersive interactions until an equilibrium layer thickness is reached. This layer is rigid, and the thickness (~5 nm) is slightly smaller than the radius of gyration of the unperturbed polymer chain (~10 nm). A flat molecular conformation of the adsorbed layer of pNIPAAm was also suggested by Plunkett et al.,[38] where they adsorbed pNIPAAm linear chains on a hydrophobized gold surface. Although the polystyrene surface is not as hydrophobic as their gold surface, it is likely that a similar phenomenon takes place here. When the polymer concentration becomes larger, approaching the overlap concentration c*, the polymer chains from the bulk start to entangle with the initial adsorbed layer, which leads to a formation of a more viscoelastic layer (Figure 12a)

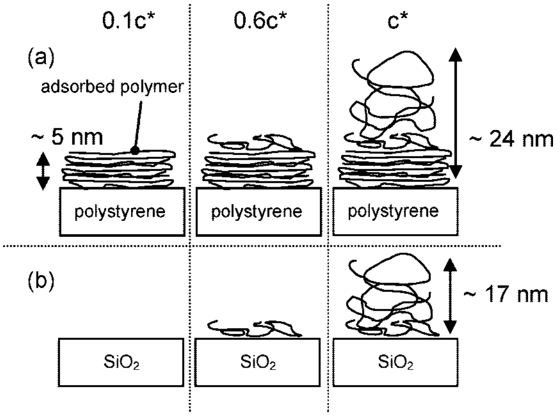

Figure 12. Schematic adsorption process of pNIPAAm chains from the bulk solutions ($0.1c^*$, $0.6c^*$, and c^*) to (a) the polystyrene, and (b) the silicon dioxide flat surfaces. On the polystyrene, pNIPAAm forms rigid adsorbed layer with a flat conformation at low bulk concentrations, followed by a viscoelastic layer at high bulk concentration. On the silicon dioxide, pNIPAAm adsorbs only at relatively higher bulk concentrations, and the adsorbed layer is viscoelastic.

For the silicon dioxide surface, on the other hand, initial formation of a rigid film is not observed, presumably because of the weaker interaction via hydrogen bonds. At higher concentration above $0.3c^*$, some polymer chains start to adsorb on the silicon dioxide, and this layer is viscoelastic, as seen from tan δ_f and ΔD data. This means that the interaction between pNIPAAm and silicon dioxide is weaker than for polystyrene. At higher concentration, the polymer adsorbs on the silicon dioxide surface, but the overall adsorbed polymer is softer than that on polystyrene (Figure 12b).

The strong adsorption of pNIPAAm chains on the polystyrene was suggested by topological effects from synchrotron SAXS and by dispersive interactions from QCM-D measurements. On the other hand, the chains loosely bind to the silicon dioxide surface, presumably via hydrogen bonds, and the flexibility of the adsorbed layer leads to additional energy dissipation in the nanocomposite. In this way, bulk viscoelastic properties of the particle-filled hydrogels have been explained by the molecular conformation of the polymer in the vicinity of the phase boundary.

Summary

We have studied the effects of the particle agglomeration and the particle−polymer affinity on the mechanical properties of particle-filled hydrogels. The effects of these two interactions were separated by utilizing the PCCA, which was originally developed by Asher et al.[6−13] We took advantage of this quasi-ordered material, where particle repulsion essentially eliminates the particle agglomeration in the nanocomposite.

From the stress relaxation study of the nanocomposite, we were able to determine that the overall relaxation behavior could be decomposed into three modes, corresponding to the relaxation in the polymer−polymer, particle−polymer, and particle−particle physical interactions. Reduction of the particle agglomeration, achieved by encapsulating the ordered colloidal array, decreased the particle−particle relaxation mode, as expected.

The synchrotron SAXS study revealed larger surface roughness on the polystyrene compared to the silica particles. The larger roughness on the polystyrene induced a topological effect where the polymer chains gained more adsorption energy without losing too much conformational entropy, resulting in strong adsorption. The QCM-D study indicated that the adsorbed polymer on the polystyrene assumed a flat conformation and that the mobility of the layer was reduced by the stronger physical interaction with the polystyrene. On the silicon dioxide, the interaction with the polymer has been proven to be smaller than on the polystyrene. The results provided by synchrotron SAXS and QCM-D verified our hypothesis that the increased energy dissipation in the silica-filled hydrogels results from a flexible adsorbed layer on silica particles.

Acknowledgment. We thank Nippon Shokubai Co. Ltd. for their gift of the silica particle suspension. Portions of this research were carried out at the Stanford Synchrotron Radiation Laboratory (SSRL), a national user facility operated by Stanford University on behalf of the US Department of Energy, Office of Basic Energy Sciences. Dr. John Pople at the SSRL and Dr. Lydia-Marie Joubert at the Cell Sciences and Imaging Facility (CSIF) at Stanford University are thanked for the assistance with SAXS and SEM measurements, respectively. This work was supported by the Center on Polymer Interfaces and Macromolecular Assemblies (CPIMA), which is sponsored by the NSF-MRSEC program. M.Y. is grateful for support in the form of a fellowship from Bridgestone Corp.

References and Notes

(1) Wypych,G. *In Handbook of Fillers*, 2nd ed.; ChemTech Publishing: Toronto, Canada, 2000; p 257.
(2) Giannelis, E. P. *Adv. Mater.* **1996**, *8*, 29–35.
(3) Chen, C. H.; Mao, C. F.; Tsai, M. S.; Yen, F. S.; Lin, J. M.; Tseng, C. H.; Chen, H. Y. *J. Appl. Polym. Sci.* **2008**, *1*, 237–243.
(4) Xu, H. H. K.; Moreau, J. L.; Sun, L.; Chow, L. C. *Biomaterials* **2008**, *32*, 4261–4267.
(5) Pek, Y. S.; Gao, S.; Arshad, M. S. M.; Leck, K.; Ying, J. Y. *Biomaterials* **2008**, *32*, 4300–4305.
(6) Asher, S. A.; Holtz, J.; Liu, L.; Wu, Z. *J. Am. Chem. Soc.* **1994**, *116*, 4997–4998.
(7) Weissman, J. M.; Sunkara, H. B.; Tse, A. S.; Asher, S. A. *Science* **1996**, *5289*, 959–963.
(8) Holtz, J. H.; Asher, S. A. *Nature* **1997**, *389*, 829–832.
(9) Holtz, J. H.; Holtz, J. S. W.; Munro, C. H.; Asher, S. A. *Anal. Chem.* **1998**, *4*, 780–791.
(10) Asher, S. A.; Alexeev, V. L.; Goponenko, A. V.; Sharma, A. C.; Lednev, I. K.; Wilcox, C. S.; Finegold, D. N. *J. Am. Chem. Soc.* **2003**, *11*, 3322–3329.
(11) Reese, C. E.; Mikhonin, A. V.; Kamenjicki, M.; Tikhonov, A.; Asher, S. A. *J. Am. Chem. Soc.* **2004**, *5*, 1493–1496.
(12) Sharma, A. C.; Jana, T.; Kesavamoorthy, R.; Shi, L.; Virji, M. A.; Finegold, D. N.; Asher, S. A. *J. Am. Chem. Soc.* **2004**, *126*, 2776–2977.
(13) Goponenko, A. V.; Asher, S. A. *J. Am. Chem. Soc.* **2005**, *30*, 10753–10759.
(14) Goodwin, J. W.; Ottewill, R. H.; Parentlich, A. *J. Phys. Chem.* **1980**, *84*, 1580–1586.
(15) Pu, Z.; Mark, J. E.; Jethmalani, J. M.; Ford, W. T. *Polym. Bull.* **1996**, *37*, 545–551.
(16) Pu, Z.; Mark, J. E.; Jethmalani, J. M.; Ford, W. T. *Chem. Mater.* **1997**, *11*, 2442–2447.
(17) Bokobza, L.; Garnaud, G.; Mark, J. E.; Jethmalani, J. M.; Seabolt, E. E.; Ford, W. T. *Chem. Mater.* **2002**, *1*, 162–167.
(18) Yanagioka, M.; Frank, C. W. *Macromolecules* **2008**, *14*, 5441–5450.
(19) Strobl, G. R.; Hagedorn, W. *J. Polym. Sci.: Polym. Phys.* **1978**, *7*, 1181–1193.
(20) Snyder, R. G.; Krause, S. J.; Scherer, J. R. *J. Polym. Sci.: Polym. Phys.* **1978**, *9*, 1593–1609.
(21) Matsuoka, H.; Murai, H.; Ise, N. *Phys. Rev. B* **1988**, *3*, 1368–1375.
(22) Matsuoka, H.; Kakigami, K.; Ise, N.; Kobayashi, Y.; Machitani, Y.; Kikuchi, T.; Kato, T. *Proc. Natl. Acad. Sci. U.S.A.* **1991**, *88*, 6618–6619.
(23) Ballauff, M.; Bolze, J.; Dingenouts, N.; Hickl, P.; Poetschke, D. *Macromol. Chem. Phys.* **1996**, *197*, 3043–3066.
(24) Dingenouts, N.; Bolze, J.; Poetschke, D.; Ballauff, M. *Adv. Polym. Sci.* **1999**, *144*, 1–47.
(25) Ciccariello, S.; Sobry, R. *J. Appl. Crystallogr.* **1997**, *30*, 1026–1035.
(26) Seelenmeyer, S.; Deike, I.; Rosenfeldt, S.; Norhausen, C.; Dingenouts, N.; Ballauff, M.; Narayanan, T.; Linder, P. *J. Chem. Phys.* **2001**, *114*, 10471–10478.
(27) Zhang, J.; Hu, S.; Rieger, J.; Roth, S. V.; Gehrke, R.; Men, Y. *Macromolecules* **2008**, *12*, 4353–4357.
(28) Schaefer, D. W.; Justice, R. S. *Macromolecules* **2007**, *24*, 8501–8517.
(29) Ballauff, M. *Prog. Colloid Polym. Sci.* **1998**, *110*, 76–79.
(30) Rosenfeldt, S.; Wittemann, A.; Ballauff, M.; Breininger, E.; Bolze, J.; Dingenouts, N. *Phys. Rev. E* **2004**, *70*, 061403.
(31) Henzler, K.; Rosenfeldt, S.; Wittemann, A.; Harnau, L.; Finet, S.; Narayanan, T.; Ballauff, M. *Phys. Rev. Lett.* **2008**, *15*, 158301.

(32) Megens, M.; van Kats, C. M.; Bosecke, P.; Vos, W. L. *Langmuir* **1997**, *23*, 6120–6129.
(33) Feigin, L. A.; Svergun, D. I. In *Structure Analysis by Small-Angle X-Ray and Neutron Scattering.* Springer: New York, NY, 1987; p 350.
(34) Roe, R. *Methods of X-Ray and Neutron Scattering in Polymer Science*; Oxford University Press, Inc.: New York, NY, 2000; p 155.
(35) Kim, M. H. *J. Appl. Crystallogr.* **2004**, *37*, 643–651.
(36) Sauerbrey, G. *Z. Phys.* **1959**, *155*, 206–222.
(37) Kanazawa, K. K.; Gordon II, J. G. *Anal. Chem.* **1985**, *8*, 1770–1771.
(38) Plunkett, M. A.; Wang, Z.; Rutland, M. W.; Johannsmann, D. *Langmuir* **2003**, *17*, 6837–6844.
(39) Voinova, M. V.; Rodahl, M.; Jonson, M.; Kasemo, B. *Phys. Scr.* **1999**, *5*, 391–396.
(40) Cho, N. J.; Kanazawa, K. K.; Glenn, J. S.; Frank, C. W. *Anal. Chem.* **2007**, *18*, 7027–7035.
(41) Voinova, M. V.; Jonson, M.; Kasemo, B. *Biosens. Bioelectron.* **2002**, *10*, 835–841.
(42) Munro, J. C.; Frank, C. W. *Macromolecules* **2004**, *3*, 925–938.
(43) Rundquist, P. A.; Photinos, P.; Jagannathan, S.; Asher, S. A. *J. Chem. Phys.* **1989**, *8*, 4932–4941.
(44) Pan, G.; Kesavamoorthy, R.; Asher, A. S. *Phys. Rev. Lett.* **1997**, *20*, 3860–3863.
(45) Fujishige, S. *Polym. J.* **1987**, *19*, 297–300.
(46) Rodahl, M.; Hook, F.; Krozer, A.; Brzezinski, P.; Kasemo, B. *Rev. Sci. Instrum.* **1995**, *66*, 3924–3930.
(47) Rodahl, M.; Kasemo, B. *Sens. Actuators, B* **1996**, *1−2*, 111–116.
(48) Chang, J.; Lesieur, P.; Delsanti, M.; Belloni, L.; Bonnet-Gonnet, C.; Cabane, B. *J. Phys. Chem.* **1995**, *43*, 15993–16001.
(49) Krieger, I. M.; O'Neill, F. M. *J. Am. Chem. Soc.* **1968**, *12*, 3114–3120.
(50) Monovoukas, Y.; Gast, A. *J. Colloid Interface Sci.* **1989**, *2*, 533–548.
(51) Bateman, J. B.; Weneck, E. J.; Eshler, D. C. *J. Col. Sci.* **1959**, *14*, 308–329.
(52) Djokovic, V.; Kostoski, D.; Galovic, S.; Dramicanin, M. D.; Kacarevic-Popovic, Z. *Polymer* **1999**, *10*, 2631–2637.
(53) Wilding, M. A.; Ward, I. M. *J. Mater. Sci.* **1984**, *2*, 629–636.
(54) Sperling, L. H. In *Introduction to Physical Polymer Science*, 4th ed.; Wiley-Interscience: New York, NY, 2006; p 349.
(55) Garvey, C. J.; Parker, I. H.; Knott, R. B.; Simon, G. P. *Holzforschung* **2004**, *58*, 473–479.
(56) Tammelin, T.; Merta, J.; Johansson, L. S.; Stenius, P. *Langmuir* **2004**, *25*, 10900–10909.
(57) Rodahl, M.; Kasemo, B. *Sens. Actuators, A* **1996**, *1−3*, 448–456.
(58) Lopez, F. V.; Pauchard, L.; Rosen, M.; Rabaud, M. *J. Non-Newtonian Fluid Mech.* **2002**, *103*, 123–139.
(59) Vlassopoulos, D.; Schowalter, W. R. *J. Rheol.* **1994**, *38*, 1427–1446.
(60) Tanahashi, T.; Kawaguchi, M.; Honda, T.; Takahashi, A. *Macromolecules* **1994**, *27*, 606–607.
(61) Stokes, R. J.; Evans, D. F. In *Fundamentals of Interfacial Engineering.* Wiley-VCH, Inc.: New York, NY, 1997; *p13*.
(62) Rubinstein, M.; Colby, R. H. *In Polymer Physics*; Oxford University Press Inc.: New York, NY, 2003; p110.
(63) Hone, D.; Ji, H.; Pincus, P. A. *Macromolecules* **1987**, *10*, 2543–2549.
(64) Ji, H.; Hone, D. *Macromolecules* **1988**, *8*, 2600–2605.
(65) Ball, R. C.; Blunt, M.; Barford, W. *J. Phys. A: Math. Gen.* **1989**, *22*, 2587–2595.
(66) Baumgartner, A.; Muthukumar, M. *J. Chem. Phys.* **1991**, *5*, 4062–4070.
(67) Vilgis, T. A.; Heinrich, G. *Macromolecules* **1994**, *26*, 7846–7854.
(68) Sung, W.; Sung, J.; Lee, S. *Phys. Rev. E* **2005**, *71*, 031805.
(69) White, C. C.; Schrag, J. L. *J. Chem. Phys.* **1999**, *111*, 11192–11206.

MA802152S